Solution Processable Polytriazoles from Spirocyclic Monomers for Membrane-based Hydrocarbon Separations

Nicholas C. Bruno,[1] Ronita Mathias,[2] Guanghui Zhu,[2] Yun-Ho Ahn,[2] Neel D. Rangnekar,[3] J.R. Johnson,[3] Scott Hoy,[4] Irene Bechis,[5] Andrew Tarzia,[5] Kim E. Jelfs,[5] Benjamin A. McCool,[3] Ryan Lively,[2]* M.G. Finn[1]*

[1] School of Chemistry & Biochemistry, Georgia Institute of Technology
[2] School of Chemical & Biomolecular Engineering, Georgia Institute of Technology
[3] Corporate Strategic Research, ExxonMobil Research and Engineering, Annandale, NJ
[4] Analytical Sciences Laboratory, ExxonMobil Research and Engineering, Annandale, NJ
[5]Department of Chemistry, Imperial College London, London W12 0BZ, UK.

Abstract

The thermal distillation of crude oil mixtures is an energy intensive process conducted on massive scale worldwide. Membrane-based separations are, in principle, much more efficient in energetic terms, if useful fractions can be obtained. We describe here a family of spirocyclic polytriazoles for membrane applications prepared by a convenient step-growth method using copper-catalyzed azide-alkyne cycloaddition, providing very fast reaction rates, high molecular weights and solubilities in common organic solvents, and non-interconnected microporosity. Fractionation of whole Arabian light crude oil and atmospheric tower bottoms feeds using these materials significantly enriched the low-boiling components and removed trace heteroatom and metal impurities, demonstrating opportunities to reduce the energy cost of crude oil distillation with tandem membrane processes. Membrane-based molecular separation under these demanding conditions is made possible by high thermal stability and a moderate level of dynamic chain mobility leading to transient interconnections between micropores, as revealed by calculations of static and swollen pore structures.

*Correspondence: M.G. Finn, mgfinn@gatech.edu; Ryan Lively, ryan.lively@chbe.gatech.edu

Introduction

The initial separation of crude oil components requires ~1100 TWh/yr, roughly 1% of humanity's total energy expenditures. Nearly 100 million barrels of crude oil are processed daily, mostly by thermal distillation to separate compounds by boiling point.[1] Membrane-based separations have the potential to reduce the resulting energy requirements by differentiating molecules based on size, shape, or polarity.[2] However, solution-processable polymers that can maintain the necessary permeances and selectivites without significant swelling, plasticization, or dissolution in organic mixtures are scarce.[3,4]

Polymers of intrinsic microporosity (PIMs) are leading materials for gas separations owing to their high free volumes and interconnected pores.[5] They have been used in organic solvent separations to a limited extent, but polymer dilation under such conditions diminishes their effectiveness in size-based separation of small molecules (< 600 Da).[6,7] To begin to address these issues, we recently reported the SBAD (spirobifluorene aryl diamine) family of polymers, moderately flexible spirobifluorene-containing materials lacking the ladder cyclic bis-ether linkages characteristic of the parent **PIM-1** polymer (**Fig. 1**). These polymers exhibited much less swelling than PIM-1 and provided pockets of non-interconnected porosity. A moderate amount of chain mobility was thought to allow the porous sections to transiently connect, providing for size- and class-based molecular filtration. **SBAD-1** provided excellent fractionation of a light shale crude, enriching molecules below 170 g/mol, albeit at low (4%) stage cuts, defined as defined as the fraction of the feed that permeates through the membrane.[8]

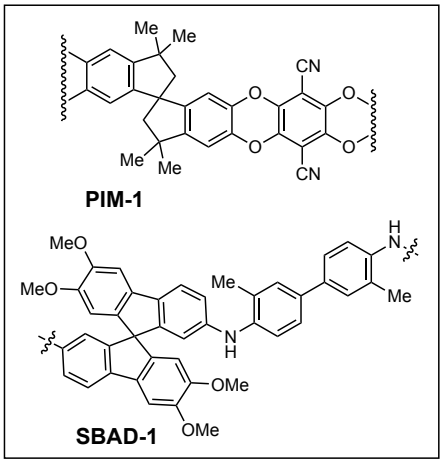

Figure 1. PIM-1 and SBAD-1 polymer structures

Click chemistry and polymer synthesis share the requirement for clean, high yielding reactions and the resulting design feature of modularity.[9,10] However, while the copper-catalyzed azide-alkyne cycloaddition reaction (CuAAC) is popular for post-polymerization functionalization, it has been used only rarely as a primary step-growth polymerization reaction. At least in part, this is due to the poor solubility generally exhibited by polytriazoles,[11-14] presumably produced by the ability of the polar aromatic 1,2,3-triazole unit to engage in both π-stacking and dipolar interactions. We reasoned that spirocyclic monomers may frustrate inter-chain interactions and thus promote solubility, allowing us to use the powerful CuAAC reaction to create triazole

analogues to the SBAD polymers of sufficiently high molecular weights to function as membrane-forming materials for liquid separations.

We describe here the synthesis and properties of a new family of such polymers with structurally diverse alkynes and azides, dubbed “DUCKY” materials in recognition of the key CuAAC reaction used to assemble them. These polymers are of high molecular weights, soluble in common organic solvents, scalable, and exhibit excellent performance as membranes for use in the fractionation of multiple crude oil feeds.

Results and Discussion

Dihydroxy-functionalized spirobisindane **2**, prepared in high yield from bisphenol A (**1**) and methanesulfonic acid,[15] served as the common starting material for the synthesis of several bis(alkyne) monomers (**Fig. 2**). Halogenation followed by propargylation provided monomers **A1** and **A2**; the more sterically-hindered **A3** was prepared analogously after electrophilic aromatic substitution with *tert*-butyl cation.[16] Lastly, the rigid bis(arylacetylene) **A4** was prepared by methylation, bromination, palladium-catalyzed Sonogashira coupling, and deprotection. Additionally, monomer **A5** was synthesized from bisphenol A to provide comparative polymers lacking a spirocenter. Benzyl azide monomers **Z1** and **Z3** were prepared from the corresponding benzyl bromides, and aryl azide monomers **Z2, Z4,** and **Z5** were prepared by Sandmeyer reaction of the corresponding anilines. All monomers were produced in decagram quantities and were purified by trituration with methanol and filtration through silica gel; column chromatography was not required. While monomers **Z1** – **Z5** and **A1 – A4** increase in steric bulk and rigidity, the CuAAC reaction was expected to be relatively insensitive to these changes, giving us the opportunity to conveniently test the relationship of monomer to polymer properties.

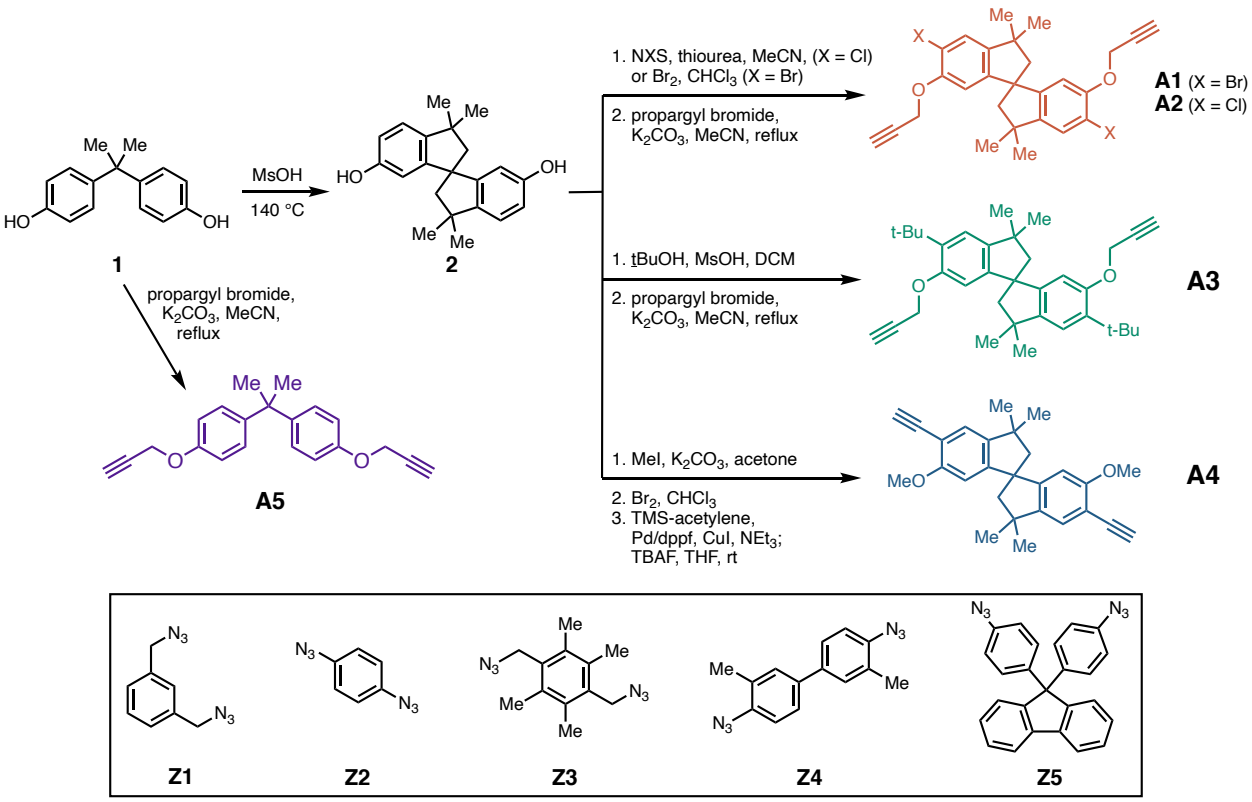

Figure 2. Dialkyne (**A1 – A5**) and diazide (**Z1 – Z5**) monomers.

The prototypical reaction of **A1** + **Z1** in chloroform (0.5 M in each monomer) was efficiently catalyzed by $(Ph_3P)_2CuOAc$ (2 mol%).[17] Initiation of the reaction by catalyst addition at room temperature resulted in a strong exotherm to the boiling point of the solvent in a matter of minutes, providing polymer **DUCKY-1** with properties characteristic of a well-behaved step-growth polymerization process (M_w = 89k, dp = 122, Đ = 2). The exclusion of water and oxygen was not necessary. These conditions were also successfully applied to all other monomer combinations except for those involving **A4**, which required higher catalyst concentration and temperature (5 mol% Cu, 0.2 M in each monomer, 60 °C) due to its greater steric hindrance. The resulting polymers (**DUCKY-1** – **DUCKY-10**) were isolated in high yields with high molecular weights and dispersities of Đ = 2 – 3 (**Fig. 3b**). With the exception of **DUCKY-2**, which was initially soluble but became insoluble in all solvents tested after isolation, all of the spirocyclic polytriazoles were freely soluble in organic solvents; in contrast, the bisphenol A-derived **BP-1** and **BP-2** (**Fig. 3b**) showed diminished solubility in chloroform.

a

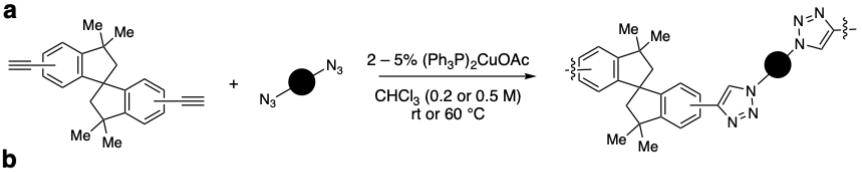

b

Polymer	Monomers	M_w	Đ	dp	T_g (°C)	T_{d5} (°C)
DUCKY-1[i]	A1 + Z1	89k	2.0	122	–	–
DUCKY-2[i]	A1 + Z2	65k	1.6	92	–	–
DUCKY-3[i]	A2 + Z1	133k	2.3	207	162	313
DUCKY-4[i]	A2 + Z3	97k	2.7	139	198	309
DUCKY-5[ii]	A4 + Z3	85k	1.7	135	n.o.	336
DUCKY-6[i]	A3 + Z3	180k	2.9	243	203	338
DUCKY-7[ii]	A4 + Z4	61k	2.4	94	n.o.	290
DUCKY-8[i]	A3 + Z4	122k	3.5	160	n.o.	268
DUCKY-9[ii]	A4 + Z5	92k	1.9	117	n.o.	272
DUCKY-10[iii]	A3 + Z5	135k	2.8	150	n.o.	302
BP-1	A5 + Z3	44k	1.9	80	–	–
BP-2	A5 + Z5	55k	3.0	78	–	–

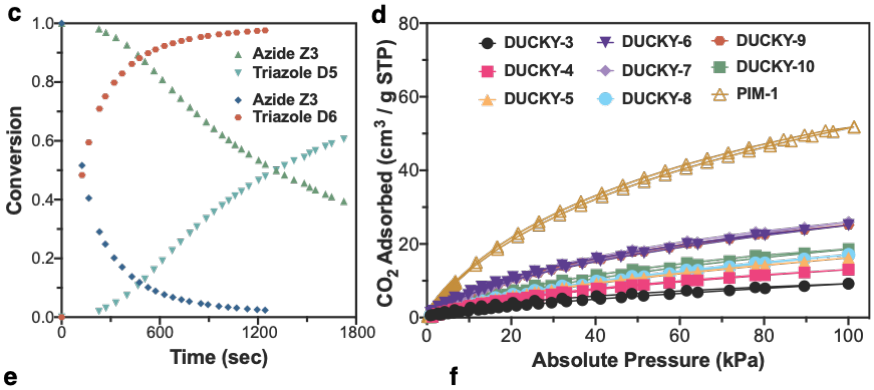

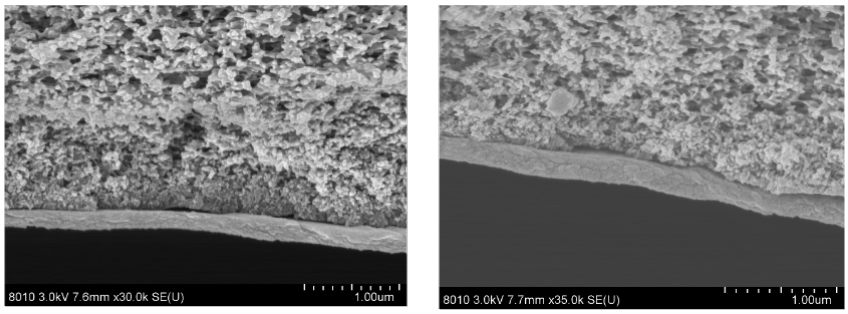

Figure 3. **Synthesis and properties of DUCKY polymers**. (**a**) General preparation. (**b**) Composition and physical characteristics. Polymerization conditions: i) 0.5 M in each monomer, 2 mol% $(Ph_3P)_2CuOAc$, 25 °C, 16 h; ii) 0.2 M in each monomer, 5 mol% $(Ph_3P)_2CuOAc$, 60 °C, 16 h; iii) 0.5 M in each monomer, 2 mol% $(Ph_3P)_2CuOAc$, 60 °C, 16 h. M_w = weight-averaged molecular weight; Đ = M_w/M_n; dp = degree of polymerization, T_g = glass transition temperature, T_{d5} = temperature at which polymer has lost 5% of its weight. "n.o." = glass transition not observed below the temperature at which decomposition began (approx. 300 °C). "–" indicates measurement was not taken. (**c**) Concentration *vs.* time data for reactions of **A4** + **Z3** (giving **DUCKY-5**) and **A3** + **Z3** (giving **DUCKY-6**) under the following conditions: $[(Ph_3P)_2CuOAc]$ = 3 μM (0.75 mol%), [monomers] = 0.2 M each, volume = 1 mL, 50 °C. The reactions were monitored by ^1H NMR; note that monomer concentration, Cu concentration, and temperature were all lower than used in bulk reactions producing the materials summarized in panel b. (**d**) CO_2 uptake at 273 K of **DUCKY** polymers and **PIM-1**.[8] (**e**) SEM image of **DUCKY-9** and (**f**) **DUCKY-10** on crosslinked polyether imide showing an approximate selective layer thicknesses of 200 nm and 250 nm, respectively.

Room-temperature ^{1}H NMR signals of all synthesized polymers with the exception of **DUCKY-9** (the most structurally rigid material) were sharp, which is unusual for high molecular weight polymers. This suggests a high degree of molecular mobility, presumably including free rotation about several C-C, C-O, and C-N bonds, aided by inhibition of inter-triazole dipole-dipole interactions by the bulky, spirocyclic monomers. Polymerization reactions involving two representative cases were therefore investigated by ^{1}H NMR at 50°C with 0.75 mol% Cu, following the disappearance of the benzyl azide protons (4.51 ppm) and appearance of benzyl triazole protons (5.72 ppm), as shown in the time-conversion plots in **Fig. 3d**. The reactions were quite rapid, the formation of **DUCKY-6** and **DUCKY-5** reaching 50% conversion in 2 minutes and 90 minutes, respectively. The difference in these examples is the nature of the alkyne, the faster reaction using propargylic **A3** rather than aryl alkyne **A4**. The same trend was noted previously for small-molecule CuAAC reactions using a different catalyst, although the reactivity difference was more dramatic here.[18,19]

The macroscopic properties of the DUCKY polymers corresponded to their anticipated rigidities. The more flexible **DUCKY-3, -4,** and **-6** exhibited glass transition temperatures from 168 to 203 °C while the more rigid **DUCKY-5, -7, -8, -9,** and **-10** showed no observable glass transition (**Fig. 3b**, **Supplementary Fig. 14**). Thermal decomposition occurred at approximately 300°C under nitrogen, somewhat lower than the thermal stabilities of **PIM-1** and **SBAD-1**. These materials exhibited low N_2 uptake capacities at 77K (**Supplementary Fig. 15**), but CO_2 sorption values at 273K of **DUCKY-3** through **DUCKY-10** were found to be in a similar range as the SBAD series, up to half that of PIM-1, and greatest in the DUCKY series for polymers derived from the arylalkyne monomer **A4** (**DUCKY-5**, **-7**, and **-9**, **Fig. 3d**). Non-spirocyclic polymers **BP-1** and **BP-2** showed no CO_2 uptake, as expected for structures lacking a spirocyclic linkage.

Thin film membrane composite membranes were fabricated by blade coating 1 wt% DUCKY polymer solutions in chloroform on cross-linked Ultem® polyetherimide supports. Scanning electron microscopy of these materials (**Fig. 3e,f Supplementary Fig. 18**) showed them to be approximately 50 – 600 nm in thickness. Their performance in molecular separations was examined by cross-flow filtration, initially on oligo(methylstyrene)s in ethanol and toluene (Supplementary **Fig. 20**). All of the DUCKY polymers surveyed outperformed **PIM-1** in solute rejection with molecular weight cutoffs of approximately 500 g/mol in both solvents, with the exception of **DUCKY-3** (cutoff of ~500 g/mol in toluene but no rejection of polystyrenes in ethanol).

DUCKY-9 and **DUCKY-10** were chosen for further evaluation as they exhibited high permeances in the range of 0.5 – 1.2 $L \cdot m^{-2} \cdot h^{-1} \cdot bar^{-1}$ for polystyrenes in toluene and very different molecular weight cutoffs. Thin-film composite membranes of these materials were challenged

with a 12-component mixture of hydrocarbons representing lower-boiling components of crude oil. In contrast to its relatively poor performance with oligostyrenes, **DUCKY-9** greatly outperformed **DUCKY-10** and gave comparable results to the commercial membrane Puramem™ 280,[8] with similar permeances and a much steeper step in rejection at 200 g/mol (**Fig. 4a,c**). It is worth noting that neither DUCKY membrane showed any rejection of pyrene (compound **7**, **Fig. 4a,c**), likely due to favorable interactions of this solute with the highly aromatic polymer. The inversion in performance of these two materials for the separation of oligostyrenes compared to the 12-component mixture in toluene suggests that **DUCKY-10** exhibits more swelling and pore dilation than **DUCKY-9** in the latter experiment. This highlights the need to test the conditions of desired separations to account for solute-membrane interactions that can dramatically influence performance.

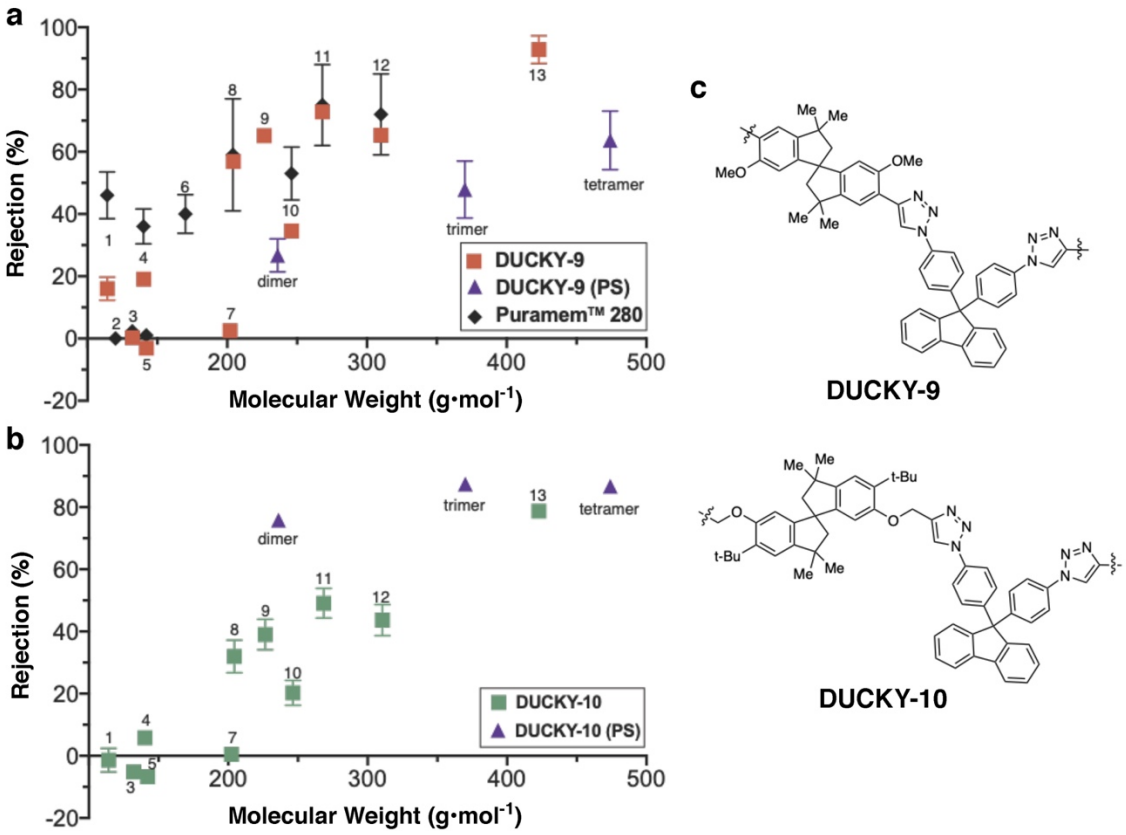

Figure 4. Dilute hydrocarbon and oligo(methylstyrene) separation performance with DUCKY-9 and DUCKY-10 thin-film composite membranes (**a**) Hydrocarbon rejections by **DUCKY-9** at 22 °C, 30 bar for a 12 component, dilute mixture (red squares, n=2), oligo(methylstyrene) standards (purple triangles, n=3), and **Puramem™-280** dilute mixture hydrocarbon rejections (black diamonds, n=3).[8] (**b**) Hydrocarbon rejections by **DUCKY-10** at 22 °C, 30 bar for a 12 component, dilute mixture (green squares, n=3) and polystyrene standards (purple triangles, n=3). (**c**) chemical structures of the **DUCKY-9** and **DUCKY-10** repeat units. Hydrocarbon mixture components, each at 1 mol% in toluene: 1) isooctane, 2) n-propylbenzene, 3) tetralin, 4) n-butylcyclohexane, 5) 1-methylnaphthalene, 6) dodecane, 7) pyrene, 8) 1,3,5-triisopropylbenzene, 9) isocetane 10) n-dodecylbenzene, 11) pristane, 12) docosane, 13) squalene.

Given its reasonably high permeance (0.23 ± 0.002 $L \cdot m^{-2} \cdot h^{-1} \cdot bar^{-1}$) with the 12-component mixture in toluene and its higher molecular weight cutoff (approx. 415 g/mol, **Supplementary Fig. 19**), we envisioned **DUCKY-9** as a good complement to **SBAD-1** (molecular weight cutoff = approx. 250 g/mol) for the enrichment of crude oil by staged filtration.[20] To explore this strategy, we challenged **DUCKY-9** membranes with an Arabian Light crude oil feed, which is significantly heavier than the shale-based light crude feed used previously with **SBAD-1**. At low stage cuts, remarkable light hydrocarbon enrichment was observed (**Fig. 5a**), albeit with low permeance (0.0014 $L \cdot m^{-2} \cdot h^{-1} \cdot bar^{-1}$). Simulated distillation[21] showed 26% of the feed to be composed of compounds boiling below 200 °C, which was enriched to 80% of the permeate at 1% stage cut and 69% for a 2% stage cut. A similar analysis for compounds boiling below 260 °C revealed enrichment from 37% of the feed to 94% and 90% of the permeate at 1% and 2% stage cuts, respectively, demonstrating excellent selectivity for molecules up to the high end of the diesel boiling range. The isolation of clear permeate from the black, molasses-like feed also illustrated a thorough removal of color bodies and higher molecular weight compounds. The 2D-GC chromatogram (**Fig. 5b)**, visualizing the differences in feed and permeate as a function of boiling point (timescale in minutes) and polarity (time scale in seconds), revealed a sharp cutoff at C_{20} (approx. 282 g/mol) with a slight bleed-through of long chain paraffinic waxes.

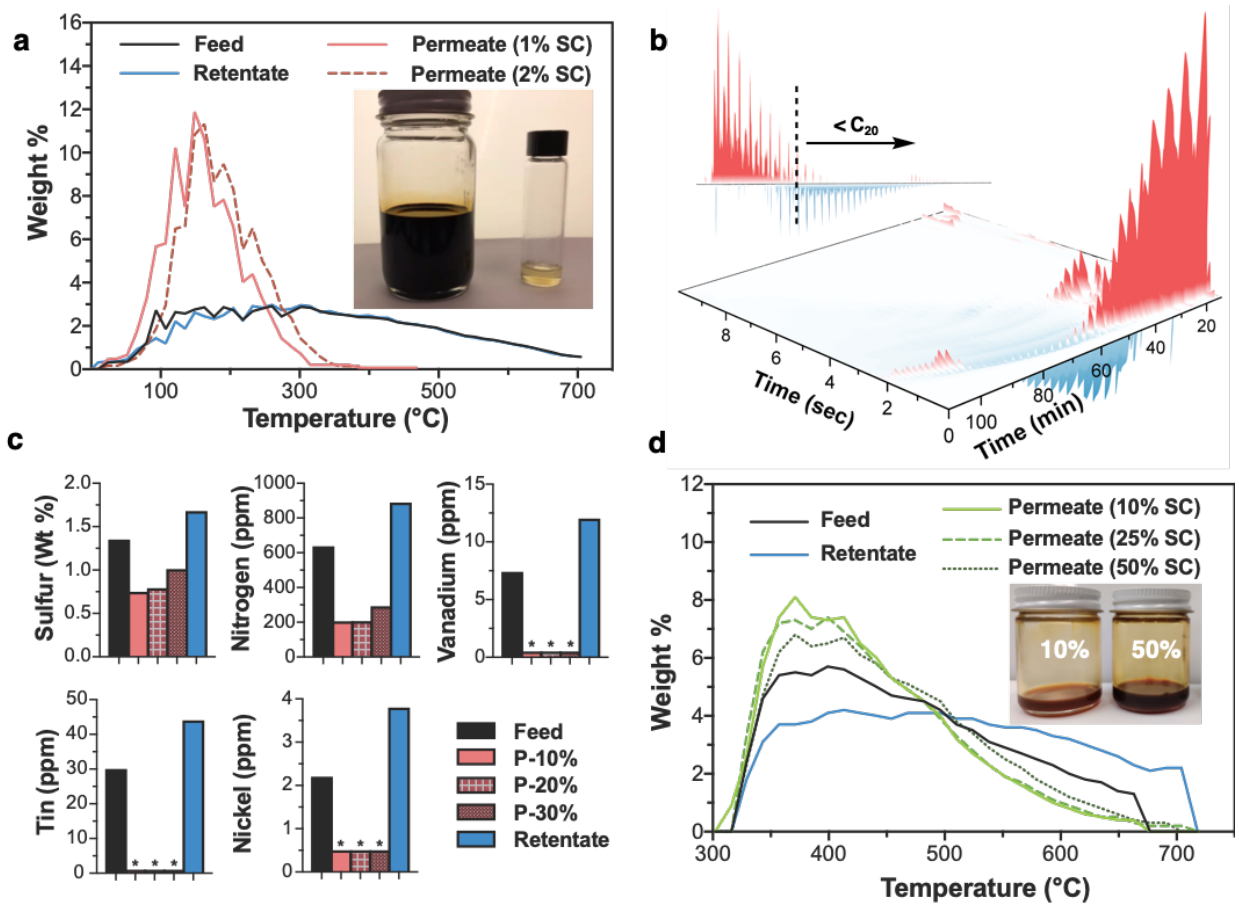

Figure 5. Enrichment of crude oil feeds with DUCKY membranes (**a**) Boiling point distribution of feed, 1% stage cut, 2% stage cut, and retentate of Arabian light crude oil fractionated with a **DUCKY-9** membrane at 130 °C, 55 bar (inset from left to right: Arabian light feed, 2% stage cut sample). (**b**) GCxGC-Flame-ionization detection (FID) analysis of **DUCKY-9** membrane fractionation of Arabian light crude oil at 130°C and 55 bar (2% stage cut) showing the feed chromatogram subtracted from the permeate chromatogram. Red elution peaks are concentrated in the permeate, whereas the blue elution peaks are concentrated in the membrane retentate, (Inset: side view of the 2D-GC spectrum shown in (**b**) with time in minutes from left to right. Dashed line indicating the approximate carbon cutoff of C_{20}.) (**c**) Elemental analysis (ICP) of Arabian light crude feed, high stage cut permeates, and retentate of the fractionation experiment in **Supplementary Fig. 22**. Asterisks indicate values below the detection limit (<0.5 ppm for V and Ni, <1 ppm for Sn). (**d**) Boiling point distribution of feed, 10%, 25%, and 50% stage cuts, and retentate for the enrichment of an ATB feed at 150 °C, 55 bar with a **DUCKY-10** membrane (inset from left to right: 10% stage cut, 50% stage cut).

Thinner membrane films (~100 nm, made from 0.75 wt% dope solution, **Supplementary Fig. 22**) exhibited increased permeance (0.025 $L \cdot m^{-2} \cdot h^{-1} \cdot bar^{-1}$), enabling us to access higher stage cuts for Arabian light crude[22] within reasonable times. At 10%, 20%, and 30% stage cuts, the permeates were visually less clear than at 2%, but still quite distinct from the feed (**Supplementary Fig. 22**). These cuts also exhibited very good enrichment with nearly identical profiles at 10 and 20 percent stage cuts: i.e., 63% of the permeate boiled below 260 °C (enriched from 44% of the feed for the samples used) and 72% boiled below 300 °C (enriched from 54% of

the feed). At a 30% stage cut, performance declined but still showed enrichment from the feed. Additionally, heteroatoms such as nitrogen,[23] sulfur,[24] and heavy metals[25] in the form of porphyrin complexes represent impurities that need to be removed from crude oil, often through expensive hydrogenation processes. Membrane filtration of Arabian light with **DUCKY-9** removed roughly half of the sulfur and two-thirds of the nitrogen, and drove nickel, tin, and vanadium to below detectable levels in all three permeate fractions (**Fig. 5c)**.

"Atmospheric tower bottoms" (ATB) represents the heaviest distillation cut from atmospheric distillation towers in oil refining. This material typically boils above ~325 °C and cannot be distilled at atmospheric pressure as many of the molecules begin to crack before vaporizing. ATB is further refined by distillation under vacuum, an energy-intensive process, to separate higher value vacuum gas oil from lower value asphalt. If a significant portion of the vacuum gas oil could be separated by membrane filtration, this would debottleneck and greatly reduce the energy duty of the vacuum crude distillation column (**Supplementary Fig. 25**).[26] To our knowledge, only one membrane-based filtration treatment of ATB material has been previously reported.[27]

At 140 °C and 55 bar, **DUCKY-9** provided modest rejections with a permeance of 0.0145 L • m^{-2} • h^{-1} • bar^{-1} for an ATB feed at a 10% stage cut and no rejections at higher stage cuts (**Supplementary Fig. 23**). **DUCKY-10**, with higher molecular weight cut-off and permeance properties, was better suited to this challenge (**Fig. 5d)**. At stage cuts of 10%, 25%, and 50%, the composition of the feed boiling below 510°C was enriched to 81%, 79%, and 75%, respectively, from a value of 66% for the feed with a permeance of 0.011 L•m^{-2}•h^{-1}•bar^{-1}, a reasonable value given the low viscosity of the feed. Additionally, the sulfur and metal contents were reduced in all three stage cuts (**Supplementary Table 6**). While the feed and retentate were very viscous liquids, the 10%, 25%, and 50% stage cuts permeates were solids at room temperature, indicating a substantial enrichment in waxes.

To help rationalize their different separation performances, we computationally modeled the pore networks of **PIM-1**, **SBAD-1**, **DUCKY-9**, and **DUCKY-10** (details in the Supplementary Information). We expected our analysis of rigid models to underestimate the interconnectivity of the pores since this method omits consideration of polymer dynamics upon adsorption/separation. In terms of pore accessibility, **DUCKY-9** and **DUCKY-10** were very similar to **SBAD-1** and showed less interconnected porosity than **PIM-1**: the largest spheres calculated to be able to pass through the materials were 3.18 (0.34), 2.30 (0.08), 2.17 (0.06) and 2.11(0.01) Å in diameter for **PIM-1**, **SBAD-1**, **DUCKY-9** and **DUCKY-10** models, respectively (Supplementary **Fig. 29a** and **Supplementary Table 11**).

The **DUCKY-9** model showed bigger pockets than **DUCKY-10** and **SBAD-1**, with the largest spheres that can fit in the pores having diameters of 9.02 (1.56) Å, 6.45 (0.13) Å, 6.64 (0.76) Å, and 10.53 (1.70) Å for **DUCKY-9**, **DUCKY-10**, **SBAD-1**, and **PIM-1**, respectively (**Supplementary Fig. 29a** and **Supplementary Table 11**). Furthermore, **DUCKY-9** has more accessible pore surface area than **DUCKY-10** (**Fig. 6a, Supplementary Fig. 29b, Supplementary Fig. 31**), the former being very similar to **SBAD-1**, and much less accessible than **PIM-1**. The calculated total surface area values for a probe of the same kinetic diameter as CO_2 (**Supplementary Table 11**) show the trend **PIM-1** > **DUCKY-9** > **SBAD-1** > **DUCKY-10**. The same trend was observed in the experimental CO_2 sorption results. Similarly, the pore size distribution of these models (2 Å diameter probe), showed pores between 2 and 7-8 Å for **DUCKY-10** and **SBAD-1**, and broader distributions between 2 and 11-12 Å for **DUCKY-9** and **PIM-1** (**Fig. 6b**). The greater porosity of **DUCKY-9** compared to **DUCKY-10** in the dry state is potentially a result of increased chain flexibility (number of rotatable bonds) of the latter and thereby opportunities for more efficient packing. The increased flexibility of **DUCKY-10** compared to **DUCKY-9** is shown by a broader distribution of the triazole-involving dihedral angles (**Fig. 6c, Supplementary Fig. 30a**).

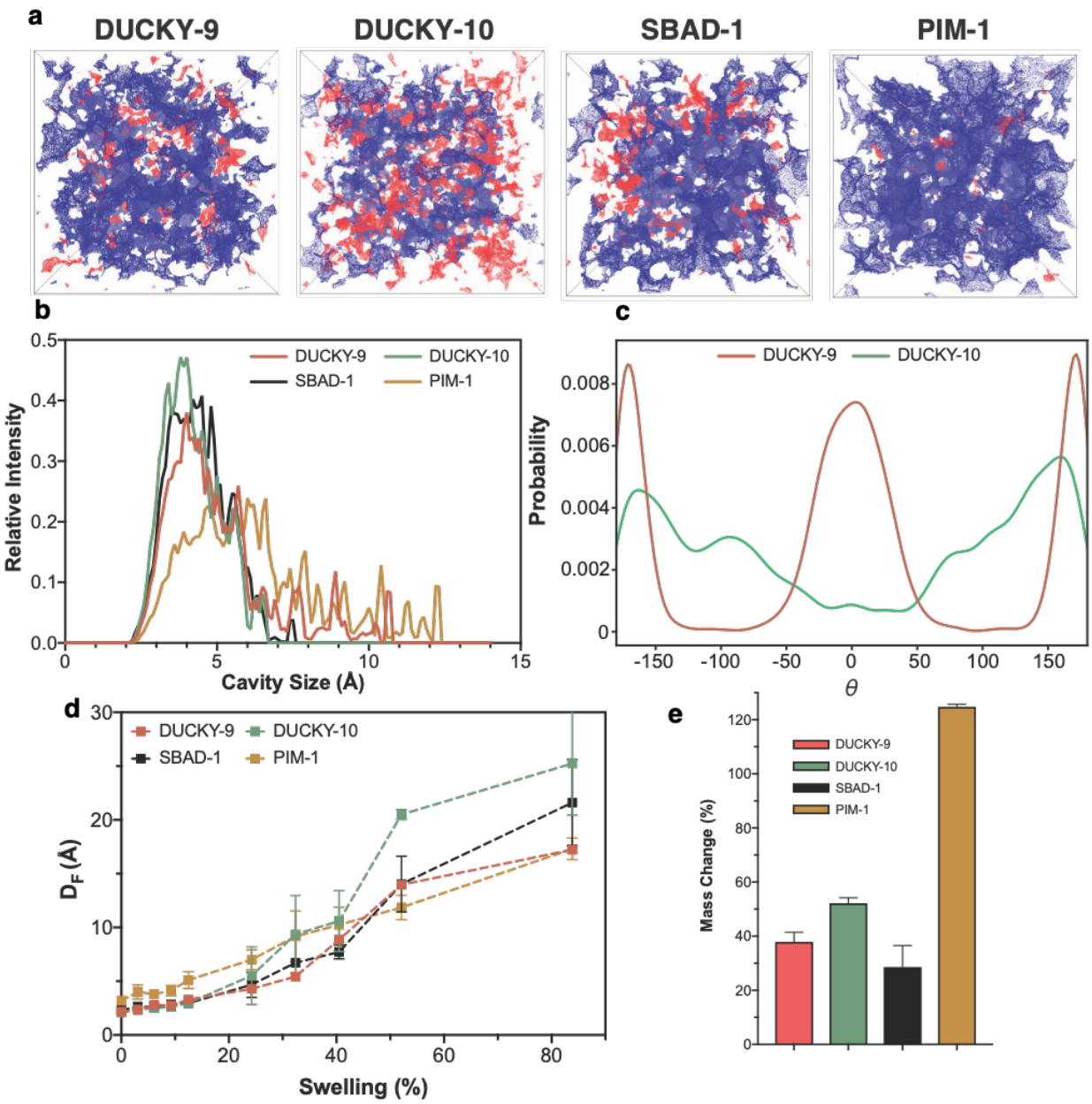

Figure 6. Molecular modelling of DUCKY polymers. (**a**) representative pore structures for **DUCKY-9**, **DUCKY-10**, **SBAD-1**, and **PIM-1** with a 2 Å diameter probe. Blue indicates interconnected surface area and red indicates non-interconnected surface area. (**b**) Calculated pore size distribution in indicated polymers. (**c**) Calculated dihedral angles in **DUCKY-9** and **DUCKY-10** about the triazole linkage (**Fig. S30a**). (**d**) Diameters of the biggest sphere that can percolate the polymer models as a function of swelling percentage. (**e**) Experimental solvent uptake for **DUCKY-9** (toluene, $N = 4$) and **DUCKY-10** (12 component mixture, $N = 4$), **SBAD-1**[8] (toluene, $N = 2$) and **PIM-1**[8] (toluene, $N = 2$). A 12-component mixture was used for **DUCKY-10** as it was somewhat soluble in toluene.

However, **DUCKY-9** showed a significantly sharper cut-off at lower molecular weights than **DUCKY-10** in the 12-component mixture separation, suggesting that calculations of dry-state structure are insufficient to fully rationalise the observed behaviour in the wet state; both the

kinetic and thermodynamic aspects of solvent-induced plasticization and swelling must be considered. To shed light on these factors, we artificially imposed different levels of swelling to the polymer models using the procedure developed by Colina and co-workers.[28] Geometrical characterisation of the porosity in the swollen models revealed that when swollen more than 20%, the diameter of the biggest sphere that can percolate the model (D_f) and the diameter of the biggest pore along the D_f path (D_{if}) are both higher for **DUCKY-10** than for **DUCKY-9** (**Fig. 6d**, **Supplementary Fig. 32a,c**). Furthermore, the porosity of **DUCKY-10** is predicted to change faster in swelling, especially at values greater than 20% (**Supplementary Fig. S32b,d**). We suggest that the more flexible chains of **DUCKY-10** may allow stronger cohesion in the dry state or when the degree of swelling is relatively low (0-20%), while allowing the structure to open more at higher degrees of swelling, as indicated in the experimental swelling results in **Fig. 6e**.

Conclusions

Organic-phase copper-catalyzed azide-alkyne cycloaddition was shown to be a convenient and scalable way to prepare porous materials using a spirocyclic bis(alkyne) and a variety aromatic and benzylic diazides. Unlike many previously reported polytriazoles, these polymers exhibited high molecular weights and solubilities in a range of organic solvents, making them well suited for solution-phase processing into membranes for molecular-scale separations. The polymerization reaction is fast, performed in air, and requires only monitoring of the reaction exotherm to ensure safe and reliable operation.

The resulting materials expand our exploration of semi-flexible spirocyclic polymers for membrane-based liquid separations.[8] These polymers share with PIMs (polymers of intrinsic microporosity) the use of spirocyclic building blocks but not rigid ladder-type linkages. As a result, SBAD and DUCKY polymers therefore do not possess interconnected microporosity, but rather have enough chain mobility to allow for the dynamic connection of large microporous void spaces. Importantly, however, the extent of chain mobility is not enough to enable large-scale swelling that would eliminate the capacity for solute size discrimination. The polytriazole DUCKY series seems to have a greater degree of solvent dependence in this regard than the SBAD materials, consistent with a greater number of rotatable single bonds in the polymer backbone. Indeed, while the incorporation of dynamic chain motion into the design and function of polymer membranes allows for new structures like the DUCKYs to be used, additional attention must be paid to the properties of the feed mixture, as different degrees of polarity and aliphatic-vs-aromatic composition can change membrane performance.

The 1,2,3-triazole unit is advantageous in these materials for its pseudo-aromatic nature and its extraordinary thermal and oxidative stability. While studies of fouling and long-term membrane aging were outside the scope of this work, membranes made from these materials are anticipated to be highly stable over time, even at the elevated temperatures required for the separation of highly viscous feedstocks such as crude oil. We also continue the exploration of the concept of multi-stage membrane separations of highly complex hydrocarbon mixtures using two or more DUCKY materials made in the same way from different components. The modular approach demonstrated here should enable the creation of tailor-made materials satisfying demanding performance criteria of size- and class-based separations, improved permeances, and staging to optimize energy savings.

References

1 International Energy Agency, "World Balance IEA Sankey Diagram" (IEA, 2018).

2 Sholl, D. S. & Lively, R. P. Seven chemical separations to change the world. *Nature* **532**, 435-437, doi:10.1038/532435a (2016).

3 Marchetti, P., Peeva, L. & Livingston, A. The Selectivity Challenge in Organic Solvent Nanofiltration: Membrane and Process Solutions. *Annu. Rev. Chem. Biomol. Eng.* **8**, 473-497, doi:10.1146/annurev-chembioeng-060816-101325 (2017).

4 Bye, K. P. *et al.* Pure and mixed fluid sorption and transport in Celazole® polybenzimidazole: Effect of plasticization. *J. Membr. Sci.* **580**, 235-247, doi:10.1016/j.memsci.2019.03.031 (2019).

5 McKeown, N. B. & Budd, P. M. Polymers of intrinsic microporosity (PIMs): organic materials for membrane separations, heterogeneous catalysis and hydrogen storage. *Chem. Soc. Rev.* **35**, 675-683, doi:10.1039/b600349d (2006).

6 Cook, M., Gaffney, P. R. J., Peeva, L. G. & Livingston, A. G. Roll-to-roll dip coating of three different PIMs for Organic Solvent Nanofiltration. *J. Membr. Sci.* **558**, 52-63, doi:10.1016/j.memsci.2018.04.046 (2018).

7 Jue, M. L., McKay, C. S., McCool, B. A., Finn, M. G. & Lively, R. P. Effect of Nonsolvent Treatments on the Microstructure of PIM-1. *Macromolecules* **48**, 5780-5790, doi:10.1021/acs.macromol.5b01507 (2015).

8 Thompson, K. A. *et al.* N-Aryl-linked spirocyclic polymers for membrane separations of complex hydrocarbon mixtures. *Science* **369**, 310-315, doi:10.1126/science.aba9806 (2020).

9 Kolb, H. C., Finn, M. G. & Sharpless, K. B. Click Chemistry: Diverse Chemical Function from a Few Good Reactions. *Angew. Chem. Int. Ed.* **40**, 2004-2021 (2001).

10 Hawker, C. J., Fokin, V. V., Finn, M. G. & Sharpless, K. B. Bringing Efficiency to Materials Synthesis: The Philosophy of Click Chemistry. *Aust. J. Chem.* **60**, doi:10.1071/ch07107 (2007).

11 Kantaria, T. *et al.* New 1,2,3-Triazole Containing Polyesters via Click Step-Growth Polymerization and Nanoparticles Made of Them. *Int. J. Polym. Sci.* **2018**, 1-14, doi:10.1155/2018/6798258 (2018).

12 Zhou, X. a. *et al.* Synthesis and characterization of novel polytriazoleimides by CuAAC step-growth polymerization. *Polym. J.* **42**, 216-222, doi:10.1038/pj.2009.337 (2010).
13 Binauld, S. *et al.* Kinetic study of copper(I) ‐ catalyzed click chemistry step ‐ growth polymerization. *J. Polym. Sci. A Polym. Chem.* **46**, 5506-5517, doi:10.1002/pola.22871 (2008).
14 Huang, D., Liu, Y., Qin, A. & Tang, B. Z. Structure–Property Relationship of Regioregular Polytriazoles Produced by Ligand-Controlled Regiodivergent Ru(II)-Catalyzed Azide–Alkyne Click Polymerization. *Macromolecules* **52**, 1985-1992, doi:10.1021/acs.macromol.8b02671 (2019).
15 Ma, X. *et al.* Synthesis and Gas Transport Properties of Hydroxyl-Functionalized Polyimides with Intrinsic Microporosity. *Macromolecules* **45**, 3841-3849, doi:10.1021/ma300549m (2012).
16 Lin, X., Zhou, Q., Pan, R. & Shan, H. Synthesis and Optical Resolution of 3,3,3′ ,3′ -Tetramethyl-1,1′ -spirobiindane-7,7′ -diol. *Synthesis* **51**, 557-563, doi:10.1055/s-0037-1610831 (2018).
17 Gonda, Z. & Novak, Z. Highly active copper-catalysts for azide-alkyne cycloaddition. *Dalton Trans.* **39**, 726-729, doi:10.1039/b920790m (2010).
18 Kislukhin, A. A., Hong, V. P., Breitenkamp, K. E. & Finn, M. G. Relative performance of alkynes in copper-catalyzed azide-alkyne cycloaddition. *Bioconjugate Chem.* **24**, 684-689, doi:10.1021/bc300672b (2013).
19 Rodionov, V. O., Presolski, S. I., Gardinier, S., Lim, Y. H. & Finn, M. G. Benzimidazole and related ligands for Cu-catalyzed azide-alkyne cycloaddition. *J. Am. Chem. Soc.* **129**, 12696-12704, doi:10.1021/ja072678l (2007).
20 McCool, B. A. J., Yogesh V.; Bhandari, Dhaval A.; Garcia, Roberto; Partridge, Randall D. . Methods for separating wax products from hydrocarbon feedstreams. US20190390126 (2019).
21 Villalanti, D. C., Fuchs, K. A. & Dowling, D. C. in *Encyclopedia of Analytical Chemistry: Applications, Theory and Instrumentation* (John Wiley & Sons, Ltd., 2018).
22 It is important to point out that though both low stage cut and high stage cut experiments used Arabian light crude oil as the feed, the two crudes were sourced from different wells and thus the feed boiling point distributions are slightly different in the separations depicted in 5a and 5d.
23 Prado, G. H. C., Rao, Y. & de Klerk, A. Nitrogen Removal from Oil: A Review. *Energy & Fuels* **31**, 14-36, doi:10.1021/acs.energyfuels.6b02779 (2016).
24 Javadli, R. & de Klerk, A. Desulfurization of heavy oil. *Appl. Petrochem. Res.* **1**, 3-19, doi:10.1007/s13203-012-0006-6 (2012).
25 Ali, M. F. & Abbas, S. A review of methods for the demetallization of residual fuel oils. *Fuel Process. Technol.* **87**, 573-584, doi:10.1016/j.fuproc.2006.03.001 (2006).
26 See Supplementary Fig. 24 for a schematic of a membrane-based atmospheric tower bottoms separation concept and example of energy savings in a process at a 50% stage cut.
27 McCool, B. A., Bhandari, D. A. & Joshi, Y. V. Boiling free fractionation of hydrocarbon steams utilizing a membrane cascade. US11084985B2 (2019).
28 Hart, K. E., Springmeier, J. M., McKeown, N. B. & Colina, C. M. Simulated swelling during low-temperature N2 adsorption in polymers of intrinsic microporosity. *Phys. Chem. Chem. Phys.* **15**, 20161-20169, doi:10.1039/c3cp53402b (2013).

29 Abbott, L. J., Hart, K. E. & Colina, C. M. Polymatic: a generalized simulated polymerization algorithm for amorphous polymers. *Theor. Chem. Acc.* **132**, doi:10.1007/s00214-013-1334-z (2013).
30 Sun, H. Force field for computation of conformational energies, structures, and vibrational frequencies of aromatic polyesters. *J. Comput. Chem.* **15**, 752-768, doi:10.1002/jcc.540150708 (1994).
31 Thompson, A. P. *et al.* LAMMPS - a flexible simulation tool for particle-based materials modeling at the atomic, meso, and continuum scales. *Computer Physics Communications* **271**, doi:10.1016/j.cpc.2021.108171 (2022).
32 Willems, T. F., Rycroft, C. H., Kazi, M., Meza, J. C. & Haranczyk, M. Algorithms and tools for high-throughput geometry-based analysis of crystalline porous materials. *Microporous Mesoporous Mater.* **149**, 134-141, doi:10.1016/j.micromeso.2011.08.020 (2012).

Acknowledgments
This work was supported by ExxonMobil Research and Engineering. We thank Prof. A. Livingston (Queen Mary University of London) for generously providing cross-linked Ultem supports, Y. Feliachi for assistance with **DUCKY-9** oligostyrene rejection measurements, A. Roy for assistance with CO_2 physadsorption measurements, and M. Rivera and Y.J. Lee for SEM images. K.E.J. acknowledges the Royal Society University Research Fellowship and a 2018 Enhancement Grant and the European Research Council (ERC) under FP7 (CoMMaD, ERC grant no. 758370).

Author Contributions
Monomer and polymer synthesis, gel permeation chromatography, spectroscopic characterization, and DSC were conducted by N.C.B. Polymer model generation and analyses were carried out by I.B., A.T., and K.E.J. Blade coating, TGA, gas physisorption, and physisorption model fitting were conducted by R.M. Oligostyrene rejections were conducted by R.M., G.Z., and Y.A. Dilute mixture separations were conducted by R.M. and N.C.B. Whole crude separations were conducted by N.R. and J.R.J. GCxGC analysis was conducted by S.J.H. The research was conceived by R.P.L. and M.G.F. N.C.B. prepared the manuscript with input from all of the authors.

Additional Information
Supplementary information is available in the online version of the paper. Reprints and permissions information is available online at www.nature.com/reprints. Publisher's note: Springer Nature remains neutral with regard to jurisdictional claims in published maps and institutional affiliations. Correspondence and requests for materials should be addressed to M.G.F. N.C.B, R.M., R.P.L., and M.G.F. are inventors on patent applications (WO2021041162A1, US20190275469, US20190390126) submitted by Georgia Tech Research Corporation and ExxonMobil Research and Engineering that covers DUCKY polymers, membrane fabrications, and crude-oil fractionation applications. All data needed to evaluate the conclusions in the paper are present in the paper or the supplementary materials.

Competing Financial Interests
The authors declare no competing financial interests.

Methods

Full details of the materials and methods, monomer synthesis, polymer synthesis, polymer model generation and analysis, powder characterization, membrane fabrication, spectroscopic characterization, and separation performance are in the supplementary information.

Synthesis of DUCKY-9: A solution of **A4** (769 mg, 2 mmol, 1 equiv.), **Z4** (801 mg, 2 mmol, 1 equiv) and bis(triphenylphosphine) copper (I) acetate (26 mg, 0.02 mmol, 2 mol %) in chloroform (10 mL) was stirred at 60 °C overnight. The solution was diluted with chloroform (5 mL) precipitated into vigorously stirring methanol (500 mL), filtered, and dried in a vacuum oven at 60 °C overnight to provide the title compound as an amber-colored solid. **Yield:** 1.51 g, 96%. GPC ($CHCl_3$, RI): M_w = 42 kDa, Đ = 2. ^{1}H NMR (500 MHz, $CDCl_3$) δ 8.34 (d, *J* = 68.1 Hz, 2H), 7.79 (d, *J* = 62.9 Hz, 3H), 7.40 (d, *J* = 44.8 Hz, 5H), 6.48 (s, 1H), 3.81 (s, 3H), 2.41 (d, *J* = 46.6 Hz, 2H), 1.45 (s, 6H) ppm. ^{13}C NMR (126 MHz, $CDCl_3$) δ 155.96, 151.62, 150.12, 145.95, 145.09, 144.25, 140.14, 136.13, 129.30, 128.08, 125.88, 121.23, 120.66, 120.51, 118.30, 106.57, 64.84, 59.72, 58.30, 55.71, 43.18, 31.67, 30.50 ppm.

Synthesis of DUCKY-10: A solution of **A3** (887 mg, 1.79 mmol, 1 equiv.), **Z4** (715 mg, 1.79 mmol, 1 equiv) and bis(triphenylphosphine) copper (I) acetate (23, 0.036 mmol, 2 mol %) in chloroform (9 mL) was stirred at 60 °C overnight. The solution was diluted with chloroform (5 mL) precipitated into vigorously stirring methanol (250 mL), filtered, and dried in a vacuum oven at 60 °C overnight to provide the title compound as an off-white solid. **Yield:** 880 mg, 98%. GPC ($CHCl_3$, RI): M_w = 135 kDa, Đ = 2.8. ^{1}H NMR (500 MHz, $CDCl_3$) δ 7.93 (d, *J* = 3.7 Hz, 2H), 7.84 – 7.77 (m, 2H), 7.60 (d, *J* = 8.3 Hz, 4H), 7.45 – 7.29 (m, 10H), 7.11 (s, 2H), 6.48 (s, 2H), 5.13 (s, 4H), 2.35 (d, *J* = 13.2 Hz, 2H), 2.27 (d, *J* = 13.0 Hz, 2H), 1.42 (s, 24H), 1.36 (s, 6H) ppm. ^{13}C NMR (126 MHz, $CDCl_3$) δ 156.78, 149.94, 148.61, 146.16, 145.54, 144.30, 140.08, 137.38, 135.81, 129.29, 128.10, 125.82, 120.54, 120.50, 120.18, 119.88, 107.94, 64.77, 62.48, 59.86, 57.48, 43.09, 34.86, 31.66, 30.54, 30.09 ppm.

.

Polymer Model Generation: Models of **DUCKY-9** and **DUCKY-10** were generated using the well-established Polymatic[29] and 21-step annealing protocol. The structures were modelled using the polymer consistent force field (pcff)[30] in LAMMPS.[31] Atom types and further details are available in the Supporting Information. Three models per polymer were generated and compared to previously generated models of SBAD-1 and PIM-1[8]. Models were artificially swollen, using the procedure by Colina and co-workers,[28] by expanding and relaxing the annealed models at varying degrees of swelling. Analysis of polymer models was performed with Zeo++[32] on the final timestep of the annealed/swollen structure. Further details are available in the Supporting Information.

Gas Adsorption: Sorption of N_2 (at 77 K) and CO_2 (at 273 K) were measured at relative pressures ranging from 1E^{-6} to 1 bar with an ASAP 2020 (Micromeritics) analyzer (Fig. 3d, Supplementary Fig. 16). The polymer powders were degassed for 12 h under vacuum at 110 °C immediately prior to analysis.

Thin Film Composite Fabrication: Thin film composites were produced from chloroform solutions of each DUCKY polymer (1 wt%) filtered through 0.45 µm PTFE syringe filters (VWR) and chilled to 4 °C. Using a 25 µm stainless steel bar applicator (Gardco), each solution was blade-coated onto a flat crosslinked polyetherimide (Ultem) support[8] with an average pore size of 18nm. The nascent polymer film was allowed to dry overnight at room temperature in a fume hood before circular coupons with an effective surface area of 14 cm^2 were cut out for testing.

Cross flow filtration: Permeation was measured with custom-built cross flow systems (Supplementary Fig. 19) pressurized by an HPLC pump (Azura P 4.1S, Knauer). The stage cut, defined as the ratio of permeate flow rate to feed flow rate, was maintained below 5% to reduce concentration polarization effects on the feed side of the membrane; concentration polarization can reduce the observed rejection of the solute. The permeance (hydraulic permeance, L•m^{-2}•h^{-1}•bar^{-1}) was calculated by normalizing the total flux through the membrane by the applied pressure.

Polystyrene Rejection: Standardized molecular weight cutoff performance was measured using 0.05 g•L^{-1} of α-methylstyrene dimer and 0.5 g•L^{-1} each of PS 580 and PS 1090, dissolved in toluene or ethanol (1 L). Thin film composites of DUCKY polymers were tested in cross flow at 30 bar. The permeate was collected every 24 hours for at least 3 days until the rejection and permeance were steady (**Supplementary Fig. 20**). The rejections of oligomers were analyzed by high-pressure liquid chromatography (Agilent HPLC) with a UV/Vis detector set at a wavelength of 264 nm. The MWCO was determined by interpolating the rejections of the marker solutes and is defined as the smallest molecular weight that corresponds to a 90% rejection.

Twelve Component Mixture Rejection: A mixture of 11 solutes (1 mol% each, **Supplementary Table S**) in toluene was used as a probe hydrocarbon feed for the data in **Fig. 4**. The mixture was pressurized to 30 bar at a flow rate of 10 mL/min and aloquots of the permeate were analyzed every 24 h until permeance and rejection were constant. The rejection of solutes was determined using gas chromatography (Agilent 7890B) and was calculated as the difference in concentration of the solute in the feed and permeate, normalized by the concentration in the feed.

Crude Oil Fractionation: Batch separation of whole Arabian light crude using DUCKY-9 or atmospheric tower bottoms with DUCKY-10: A 49 mm diameter coupon of DUCKY-9 or DUCKY-10 was loaded into a Sterlitech HP4750X stirred dead end cell (active membrane area = 14.6 cm^2) with a custom-made heating jacket and nitrogen line for application of head pressure. The cell was initially loaded with 50g of toluene which was allowed to permeate overnight at room temperature and 800 psig N_2 head pressure. The cell was then depressurized and loaded with 100 g of Arabian light whole crude oil or atmospheric tower bottoms and 800 psig N_2 head pressure was again applied. The cell was stirred at a constant rate of 400 rpm. A cold trap cooled by dry ice was set up to collect the permeate in order to prevent loss of the light ends. The temperature of the cell was slowly increased up to 130 °C (Arabian light crude) or 140 °C (ATB) until permeate flow was observed. After sufficient permeate had been collected, the cell was cooled and depressurized. The permeate, retentate and feed samples were analyzed using simulated distillation (SIMDIS) and, for Arabian light crude, 2-dimensional gas chromatography (GCxGC).

Two-Dimensional Gas Chromatography: The GCxGC system consisted of an Agilent 6890 gas chromatograph (Agilent Technologies, Wilmington, DE) configured with a split/splitless inlet, oven, and flame ionization detector, and a Zoex ZX1 looped jet thermal modulation assembly (Zoex Corp., Houston, TX). The column system was a combination of three different columns connected in series. The first column was a weakly-polar BPX-5 (30 m length, 0.25 mmID, 0.25 µm film), followed by an intermediate- polarity BPX-50 (1.5 m length, 0.1 mmID, 0.1 µm film) interface column, and an additional intermediate-polarity BPX-50 (1.9 m length, 0.1 mmID, 0.1 µm film) analytical column. All columns were purchased from SGE Analytical (SGE Analytical Science, Austin, TX). The ZX1 modulator uses a combination of alternating cold and hot nitrogen gas jets regulated by liquid nitrogen heat-exchange and electric auxiliary heating to trap and release “slices” of eluent from the first column onto the second column. This trapping occurs on the interface column which is looped through the intersection of both gas jets in the oven. A 2.0 µL sample was injected neat into the split/splitless inlet with a 20:1 split ratio at 360 °C. The carrier gas was helium running in constant flow mode at 1.9 mL per minute. The oven was programmed from 60 °C to 390 °C at 3 °C per minute for a total run time of 110 minutes. The modulator hot jet is programmed from 180 °C to 390 °C at 3 °C per minute and then held for 40 minutes until the end of the run. The modulation period was 10 s with a hot jet pulse length of 400 ms. The FID sample rate was 100 Hz. Instrument control and FID data collection was conducted using Agilent Chemstation. FID signal processing was conducted using GC Image software (GC Image, LLC, Lincoln, NE). GC Image constructed the two-dimensional and three-dimensional GCxGC plot images from the Chemstation FID channel file using built-in baseline correction, peak detection, and peak integration algorithms. Three-dimensional comparison images were also constructed using built- in functionality. Due to the complexity of the Arabian light crude oil feed, the GCxGC chromatographs have too many overlapping peaks to analyze the components by molecule or by molecular class.